ELSEVIER

International Journal of Mass Spectrometry 205 (2001) 93–110

International Journal of Mass Spectrometry

Dissociative electron attachment to CCl_4 molecules at low electron energies with meV resolution

D. Klar, M.-W. Ruf, H. Hotop*

Fachbereich Physik, Universität Kaiserslautern, D-67653 Kaiserslautern, Germany

Received 23 March 2000; accepted 29 May 2000

Abstract

Using the laser photoelectron attachment (LPA) method we investigated dissociative electron attachment to carbon tetrachloride [$e^-(E) + CCl_4 \rightarrow Cl^- + CCl_3$] in the electron energy range $0 < E \leq 173$ meV with very high resolution (energy width 1 meV). With reference to a reliable thermal electron attachment rate coefficient $k_e(T = 300\ K)$ absolute values for the attachment cross section $\sigma_e(E)$ are derived. The $\sigma_e(E) \propto E^{-1/2}$ behaviour of the cross section for $E \rightarrow 0$, theoretically predicted for *s*-wave attachment to molecules without permanent electric dipole moment, is approximately reached at very low energies ($E \lesssim 0.3$ meV). Toward higher energies the cross section decreases more rapidly. At thresholds for vibrational excitation of the neutral molecule, the cross section exhibits pronounced cusp structure of downward step character due to coupling of the attachment process with scattering channels. Comparisons are made with cross sections derived from previous photoelectron attachment work and from experiments involving electron beams, electron swarms and Rydberg atoms. Combination of our LPA cross section with beam data results in a recommended total DA cross section for CCl_4 over the energy range 0–2 eV. Based on this cross section, we calculate and report the energy dependence of the rate coefficient $k_e(E)$ for monoenergetic free electron attachment and the electron temperature dependence of the rate coefficient $k_e(T_e)$ for free electron attachment involving a Maxwellian electron ensemble and CCl_4 gas at room temperature ($T_G = 300$ K). The effects of electron energy resolution on measured low energy electron attachment yields, in particular on the effective location and energy width of the "zero energy peak," are discussed in some detail. (Int J Mass Spectrom 205 (2001) 93–110) © 2001 Elsevier Science B.V.

Keywords: Electron attachment; Negative ions; Threshold law; Carbon tetrachloride

1. Introduction

The investigation of electron attachment to molecules XY and the determination of cross sections $\sigma_e(E)$ for the process:

$$e^-(E) + XY \xrightarrow{\sigma_e(E)} XY^{-*} \rightarrow X + Y^- \qquad (1)$$

[dissociative attachment (DA), short notation: Y^-/XY] have been subjects of a considerable number of studies [1–20]. Following its formation the excited, temporary anion XY^{-*} can either decay by autodetachment (corresponding to elastic or inelastic electron scattering) or it may dissociate, thereby forming stable negative ions Y^-; in some cases a long-lived complex XY^{-*} is created which can be detected mass spectrometrically (e.g. SF_6^- [4,14,16,19]). In DA processes part of the excess energy stored in the excited negative ion XY^{-*} is converted into kinetic energy of

* Corresponding author. E-mail: hotop@physik.uni-kl.de

Dedicated to Professor Aleksandar Stamatovic on the occasion of his 60th birthday.

PII S1387-3806(00)00271-2

the fragment particles. For attachment of an electron with kinetic energy E to a molecule XY, the kinetic energy E_{Y^-} of the fragment Y^- is given by

$$E_{Y^-} = (1 - m_Y/m_{XY})[E + \mathrm{EA(Y)} - D(\mathrm{XY}) - E_F] \quad (2)$$

where EA(Y) and D(XY) are the electron affinity of Y and the dissociation energy of XY, respectively. E_F represents the internal excitation energy of the fragments and m_Y and m_{XY} are the respective masses. Electron attachment experiments, motivated by a fundamental interest in the dynamics of such reactions and in the properties of negative ions, but also by practical applications like the design of gaseous dielectrics [6], include several complementary methods like electron swarms [4,6,7,9,13,15,21,22], beam experiments [1–3,5,10,18,20,23–26], electron transfer from high Rydberg atoms [16,27,28], and threshold photoionization methods producing slow photoelectrons with variable energy [8,12,14,17,19,29,30].

Electron attachment in the energy range distinctly below 1 eV is of special interest in connection with the test of quantum mechanical threshold laws [14,16,19,31] and with the investigation of cross section shapes [Wigner cusps, vibrational ("nuclear-excited") Feshbach resonances] at thresholds for vibrational excitation of the neutral target molecule [14,17,24,30–36]. For the cross section $\sigma_e(E; L)$ associated with the partial wave of orbital angular momentum L, the physics of threshold laws [31] requires the following limiting energy dependence (as long as the electron–target interaction potential is sufficiently short-ranged, i.e. $V(r) \propto r^{-m}$, $m > 2$, excluding molecules with permanent dipole moments):

$$\sigma_e(E \to 0; L) \propto E^{L-1/2} \quad (3)$$

For s-wave attachment ($L = 0$) the cross section diverges as

$$\sigma_e(E \to 0; L = 0) \propto E^{-1/2} \propto v^{-1} \quad (4)$$

For molecules without permanent electric dipole or quadrupole moments the leading long-range interaction between electron and target is the polarization potential $V(r) = -\alpha e^2/2r^4$. For this case Vogt and Wannier [37] predicted that Eq. (4) takes the explicit form (a_0 = Bohr radius = 529.177 pm, polarizability α and energy E in atomic units):

$$\sigma_c(E \to 0; L = 0) = 4\pi a_0^2(\alpha/2E)^{1/2}. \quad (5)$$

The capture cross section (5) also represents the low energy limit of a semiempirical formula suggested by Klots [38] to describe low energy electron attachment processes:

$$\sigma_K = (\pi a_0^2/2E)\{1 - \exp[-4(2\alpha E)^{1/2}]\} \quad (6)$$

which interpolates between the Vogt and Wannier formula (5) for $E \to 0$ and the s-wave reaction cross section $\pi\lambda\!\!\!^{-2} = \pi a_0^2/(2E)$ [for $4(2\alpha E)^{1/2} \gg 1$; $\lambda\!\!\!^{-}$ = reduced de Broglie wavelength] [14,30]. The Klots formula (6) has been frequently used to calculate rate coefficients for Rydberg electron attachment [16,27]. More recently, a variant of the Klots formula has been used by Klar and co-workers [14,17] for fits to their high resolution attachment cross sections obtained with the laser photoelectron attachment (LPA) method (see the following):

$$\sigma_e(E) = (\sigma_0/E)[1 - \exp(-\beta E^{1/2})]. \quad (7)$$

The parameter β characterizes the energy range ($\beta^2 E > 0.1$) above which substantial deviations from the limiting s-wave attachment behaviour $\sigma_e(E \to 0) = \sigma_0 \beta E^{-1/2}$ occur. For SF_6^- formation, use of the Klots formula (6) corresponds to choosing $\beta = 0.228$ [$\alpha(SF_6) = 44.1\ a_0^3$ [39], E in meV], whereas from their LPA experiment [14] Klar et al. determined $\beta = 0.405 \pm 10\%$ (see also [29]). We note that for molecules with permanent electric dipole moment one expects a limiting s-wave attachment cross section of the form $\sigma_e(E \to 0; L = 0) \propto E^{-x}$ with $0.5 < x < 1$ [11,16,40], i.e. a behaviour between those for capture in short range potentials ($m > 2$, $x = 0.5$) and in the Coulomb potential ($x = 1$, independent of L) [31].

In order to experimentally establish the range of validity of the threshold law a method with the highest possible energy resolution should be used. Chutjian and co-workers [8,12,19] developed the threshold photoelectron spectroscopy for attachment (TPSA) method, which involves the production of energy

variable electrons by photoionization of rare gas atoms Rg (mostly Rg = Kr) at and above the $Rg^+(^2P_{1/2})$ threshold with monochromatized VUV light, and applied it to DA of a large number of molecules at typical quoted resolutions around 6–8 meV. In our group, the LPA method [14,41] was developed and sub-meV resolution in a free electron collision experiment was demonstrated for the first time by Klar et al. [14] in a detailed study of SF_6^- formation. More recently, energies down to 20 μeV at energy widths as low as 20 μeV were achieved by Schramm et al. [29]. In order to reach sub-meV resolution a careful characterization of the residual electric field is mandatory, and for this purpose laser diagnostics at narrow bandwidths is very well suited and important [29,41]. Comparison with the TPSA data for SF_6 revealed that energy widths $\geq$5 meV are not sufficient for a detailed study of the threshold behaviour for $E \rightarrow 0$ or for the detection of cusp features at vibrationally inelastic thresholds in polyatomic molecules such as SF_6 or CCl_4 [14,17,34].

An interesting alternative to investigate electron attachment to molecules or clusters at very low energies is electron transfer from highly excited Rydberg atoms A**(nl) (abbreviated by RET) [16,27,28,42–45]:

$$A^{**}(nl) + XY \xrightarrow{k_{nl}} [A^+ - XY^{-*}]$$

$$\rightarrow A^+ + X + Y^- \qquad (8)$$

as investigated in great detail especially by Dunning and colleagues [16,27]. At high principal quantum numbers n the influence of postattachment reactions due to the Coulomb attraction of the intermediate ion pair complex $[A^+ - XY^{-*}]$ can be neglected [16,28]. Then, in the framework of the quasifree Rydberg electron model [16,27,28,46], the connection of the rate coefficients k_{nl} and k_e ($k_e = \sigma_e v_e$, v_e = free electron velocity) for Rydberg and free electron attachment is given by

$$k_{nl} = \int k_e(v)\, f_{nl}(v)\, dv \qquad (9)$$

where $f_{nl}(v)$ is the normalized Rydberg electron velocity distribution. To test the adequacy of the free electron model, experimental rate coefficients k_{nl} should be compared with values calculated from Eq. (9) on the basis of dependable and sufficiently high-resolved experimental data for k_e, taken at sufficiently high resolution and down to the lowest possible energies. In evaluating Eq. (9) [16,28] our LPA results for k_e [incorporating the fit function (7) at very low electron energies] and normalized classical distribution functions $f_{nl}(v)$ were used.

Using the LPA method, described in detail in [14,41] and summarized in Sec. 2, we have carried out a detailed investigation of dissociative free electron attachment to the carbon tetrachloride (CCl_4) molecule with very high resolution (energy width $\leq$1 meV). Similar LPA experiments have been performed on the dipolar molecules $CFCl_3$, 1,1,1-$C_2Cl_3F_3$, HI, CCl_3Br, and CH_2Br_2; these results will be published elsewhere. In Sec. 3 we present the experimental results and compare them with data of other groups. Previous work, performed at substantially larger energy widths, includes the TPSA results [8], electron beam studies [2,10,18,25,47,48] and several investigations with electron swarms [13,21,49–52]. In addition, RET studies at medium [27,53–55] and up to very high quantum numbers [16,56] have been carried out.

2. LPA method

The LPA method, its experimental parameters and the results for XY = SF_6 have been reported in detail in [14,29,41]. Here we outline the basic features and discuss some special aspects pertinent to the molecule under study. The LPA experiment involves the generation of free electrons with variable energy and narrow energy spread by photoionization of suitable atoms with a monochromatic tunable laser, in our case resonant, two-step photoionization of metastable Ar* atoms. The photoelectrons react with molecules of an ambient diffuse gas target (T_G = 300 K) [14,17,30] (or, alternatively, with molecules or clusters in a collimated target beam [29,57]) under conditions of

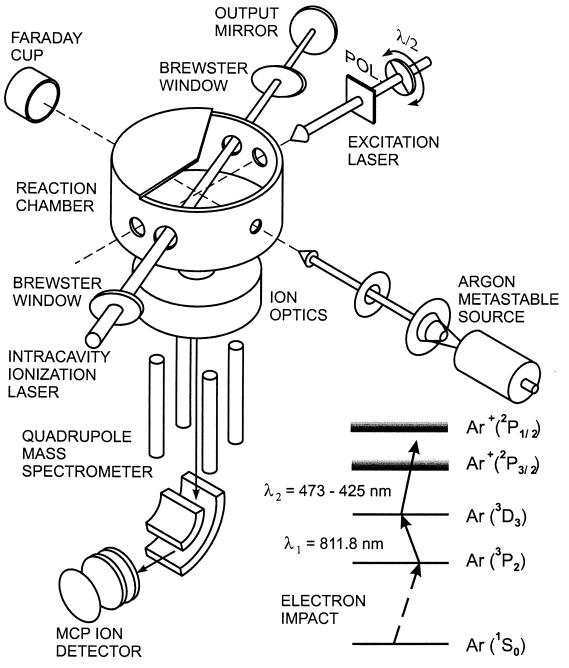

Fig. 1. Schematic setup of the laser photoelectron attachment experiment. The beam of metastable Ar*($4s\ ^3P_{0,2}$) atoms is intersected in the centre of the reaction chamber by the excitation (laser 1) and the intracavity ionization laser (laser 2). Photoelectrons of variable energy react with molecules in a diffuse gas target (phase I), and the negative product ions are extracted from the reaction chamber into the ion optics by a pulsed electric field (phase II) and mass analyzed by a quadrupole mass spectrometer. After the negative ions have passed a 90° deflection unit, they are detected by a dual microchannel plate detector in chevron arrangement.

low residual electric field ($F \leq 0.5$ V/m) and negligible magnetic field ($B < 2 \times 10^{-6}$ T). Negative ions resulting from electron attachment reactions are extracted by a pulsed electric field and analyzed by a quadrupole mass spectrometer.

The experimental setup and excitation scheme are shown in Fig. 1. A collimated beam of metastable argon atoms Ar*($4s$, $^3P_2$) is excited to Rydberg states (ns, nd) or to the ionization continuum by two lasers via the Ar*($4p$, $^3D_3$) intermediate level. A continuous wave (cw) single mode dye laser ($\lambda_1 = 811.75$ nm) transversely excites the closed transition Ar*($4s$, $^3P_2 \rightarrow 4p$, $^3D_3$) and a small fraction of the Ar*($4p$, $^3D_3$) population is excited further by a tunable intracavity dye laser (mode spacing about 40 MHz). A three plate birefringent filter as wavelength selecting element narrows the bandwidth of the laser to about 150 μeV; an additional thin etalon (free spectral range about 900 GHz) improves the bandwidth by another factor of three. Both lasers are linearly polarized with electric vectors parallel to each other and to the direction of ion extraction. By tuning the intracavity laser over the wavelength range 473–425 nm, bound Ar**(nl)-Rydberg levels ($n \gtrsim 15$, $E < 0$) or free electrons (energies $E > 0$ up to 230 meV) are created. Electron transfer from Rydberg atoms (RET) or free electron attachment processes to a diffuse molecular gas target take place in the center of a specially designed reaction chamber. The experiment is pulsed at a repetition rate of 140 kHz: a time interval of essentially field-free conditions for electron production and attachment (phase I, 2.7 μs) is followed by a period for ion extraction with a delayed pulsed electric field (23 V/cm) (phase II, 3.4 μs). During phase II the infrared laser and thereby the electron production are switched off by an acousto-optical modulator. The accelerated negative ions are imaged into a quadrupole mass spectrometer, and the mass-selected ions are detected by a dual channel plate following a 90° deflection by an electric field. Weak, energy independent background signals, e.g. dark counts of the channel plate detector and Cl^- production due to attachment reactions of electrons resulting from Penning ionization of CCl_4 in collisions with metastable Ar*($4s\ ^3P_{2,0}$) and laser-excited Ar*($4p\ ^3D_3$) atoms, were repeatedly determined by interrupting photoelectron production through insertion of a glass plate into the cavity of the ionization laser. Subtraction of this background from the total count rate yielded the negative ion signal I_e due to electron attachment. Simultaneously with I_e, the output power P_γ^{oc} of the intracavity dye laser and its transmission through a calibrated etalon is measured. The latter interference fringes establish a relative energy scale for the spectra, accurate to within 10^{-3}. Absolute energies are considered to be accurate to within ± 0.4 meV or less. Correcting the signal I_e for the wavelength dependent intracavity photon flux $F_\gamma^{ic}(E)$ and the known energy dependence of the Ar*($4p$, $^3D_3$) photoionization

Table 1
Molecular properties and electron attachment characteristics for SF_6 and CCl_4

Property	SF_6	CCl_4
α [a_0^3]	44.1[a]	75.6[a]
μ [D]	0	0
k_c [10^{-7} cm^3 s^{-1}] (Vogt, Wannier)	5.15[b]	6.74[b]
$k_e(T_e = 300$ K) [10^{-7} cm^3 s^{-1}] (electron swarms, $T_G = 300$ K)	2.27(9)[c]	3.79(19)[d]
k_{nl} [10^{-7} cm^3 s^{-1}] (RET, $T_G = 300$ K)	4(1)[e]	11(2)[f]
σ_0 [10^{-20} m^2 meV][g]	7130(360)[h]	11160(560)[i]
β [(meV)$^{-1/2}$][g]	0.405(40)[h]	0.59(6)[i]
$k_e(E \rightarrow 0)$ [10^{-7} cm^3 s^{-1}] (LPA, $T_G = 300$ K)	5.4(8)[h]	12.3(19)[i]
Energy integrated cross section [10^{-20} m^2 eV] (LPA, $T_G = 300$ K)	30.0[h,j]	53.3[i,j] 57.6[i,k]

[a] See [39].
[b] Using Eq. (15) and polarizabilities in first column (ignoring effects of other long-range electron-molecule interactions).
[c] See [7].
[d] See [51].
[e] See [54].
[f] See [56].
[g] Fit parameter in Eq. (7).
[h] See [14].
[i] Present work.
[j] Integrated from 0 to 200 meV.
[k] Integrated from 0 to 2000 meV.

cross section $Y_\gamma(E)$ [14,58] results in the negative ion yield Y_e [14,41]:

$$Y_e(E) = \frac{I_e(E)}{Y_\gamma(E)\,F_\gamma^{\mathrm{ic}}(E)} = \frac{I_e(E)}{Y_\gamma(E)}\,\frac{T(E)h\nu}{2P_\gamma^{\mathrm{oc}}(E)} \qquad (10)$$

where $T(E)$ is the wavelength dependent transmission of the terminating mirror of the intracavity laser. For $E > 0$ (free electron attachment) $Y_e(E)$ represents the relative attachment cross section, while for $E < 0$ the negative ion yield is proportional to the rate coefficient for Rydberg electron attachment [14,29]. Absolute attachment cross sections $\sigma_e(E) = NY_e(E)$ were established by normalization of the relative cross section $Y_e(E)$ to a well-known thermal energy attachment rate coefficient $k_e(T)$, obtained in electron swarm experiments at equal electron and gas temperature (i.e. $T = T_e = T_G = 300$ K, see Table 1), using the expression [8,14]:

$$k_e(T) = N\sqrt{2/m}\int_0^\infty Y_e(E)\,E^{1/2}f(E;\,T)\,dE \qquad (11)$$

with $f(E;\ T) = (2/\sqrt{\pi})\bar{E}^{3/2}\ \exp(-E/\bar{E})$ ($\bar{E} = k_BT = 25.85$ meV for $T = 300$ K). The uncertainties for $\sigma_e(E)$ given in the following sections do not include the uncertainty of the literature value for $k_e(T)$.

Carbon tetrachloride is a liquid at room temperature and standard pressure. Following pump out of the target gas line, the CCl_4 vapour was expanded into the vacuum apparatus from the vapour above the liquid surface. The gas inlet system was partly heated to prevent condensation of the vapor and to minimize pressure variations in the reaction volume. Pressure variations in the range (0–5)% were observed over the scan period of the ionizing laser. By correcting each spectrum with the registrated pressure variation and addition of several measurements to generate the final data, we reduced the overall uncertainties associated with pressure variations to below 1%. The target gas density was adjusted to values below 10^{11} cm^{-3} at low energies and to values up to 8×10^{11} cm^{-3} at higher electron energies, ensuring single collision conditions in all cases.

Electric stray fields in the reaction volume were determined through the measured shift of the $Ar^+(3p^5\ ^2P_{3/2})$ ionization threshold and model calculations to reproduce the behaviour of negative ion yield for $E \gtrsim 0$ (see the following, for details see [41]). In the present work typical stray fields amounted to $F_S \approx 0.5$ V/m (see Sec. 3); from the dimensions of the reaction volume [41] the effective energy widths for the attachment experiment is thus estimated to be $\Delta E \approx 1$ meV or below. The cross section values presented below are based on measurements over the energy interval $-40 \lesssim E \lesssim 200$ meV, carried out with an intracavity laser bandwidth ΔE_L of about 150 μeV, and data obtained for the negative ion yield close to the $Ar^+(3p^5\ ^2P_{3/2})$ ionization threshold with a photon bandwidth of 50 μeV.

A further systematic error for the dissociative processes is connected with a possible variation of the negative ion detection efficiency over the covered

electron energy range due to the fact that the kinetic energy of the negatively charged dissociation fragments depends on the energy E of the attached electron [see Eq. (2)]. The ion optical properties in the reaction chamber during the extraction period II (as previously discussed) minimize such a variation by collecting ions over an extended volume. Discrimination effects concern predominantly the negative ions created at the beginning of the electron production and attachment period I and among them mainly those moving initially perpendicular to the detection direction. By taking an average over the whole attachment period and the total detection volume, we estimate the overall variation in ion detection efficiency over the electron energy range (0–173) meV to be smaller than 10% for Cl^- production from CCl_4. We note that for the production of Cl^- from CCl_4 at low electron energies, RET studies of Dunning's group [55] (see also Sec. 3.1) have demonstrated that only a small fraction of the excess energy appears as translational energy of the DA products.

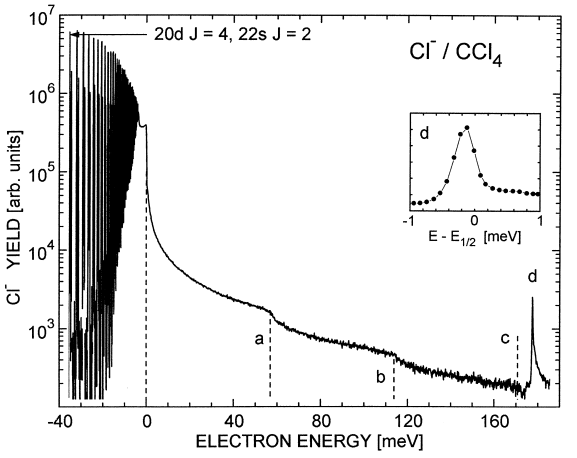

Fig. 2. Yield of Cl^- ions due to collisions of Ar**(ns, nd) Rydberg atoms ($E < 0$) and of free electrons ($E > 0$) with CCl_4 molecules (gas temperature T_G = 300 K), measured with a photon energy bandwidth of 0.15 meV (FWHM) at a residual electric field of 0.55 V/m. In the range $0 < E < 173$ meV the Cl^- yield is proportional to the dissociative attachment cross section. The downward steps a, b and c are due to channel interaction with onsets for excitation of 1, 2, and 3 quanta of the symmetric stretch vibration ν_1. The sharp peak d corresponds to Cl^- formation by very slow electrons associated with the $Ar^+(^2P_{1/2})$ threshold (see text).

3. Results and discussion

3.1. Absolute dissociative electron attachment cross sections for CCl_4

The molecule CCl_4 has T_d symmetry and possesses four distinct vibrational modes: the totally symmetric stretching mode ν_1 [A_1 symmetry, energy $E(\nu_1)$ = 56.9 meV], the doubly degenerate deformation mode ν_2 [E symmetry, $E(\nu_2)$ = 26.9 meV], the triply degenerate (asymmetric) stretching mode ν_3 [F_2 symmetry, $E(\nu_3)$ = 92.2 meV], and the triply degenerate deformation mode ν_4 [F_2 symmetry, $E(\nu_4)$ = 38.9 meV] [59]. Attachment of free electrons to CCl_4 leads to dissociation of the molecule [10]; at low energies only Cl^- ions are formed:

$$e^-(E) + CCl_4(^1A_1) \rightarrow Cl^- + CCl_3. \quad (12)$$

At low energies process (12) proceeds by s-wave electron attachment through the symmetric $CCl_4^-(^2A_1)$ resonance state [15,51], correlating to the lowest $Cl^- + CCl_3$ limit which lies about 0.6 eV [55] below the vibrational ground state of $CCl_4(^1A_1)$. At higher energies another broad peak in the total negative yield was observed at 0.8 eV and assigned to the excited $CCl_4^{-*}(^2T_2)$ state [25]. At energies above about 0.6 eV other product ions including CCl_3^-, CCl_2^-, and Cl_2^- are observed [10]. We note that the present article addresses the total electron attachment cross section.

The energy dependence of our measured Cl^- yield $Y_e(E)$ is shown in Fig. 2. For $E < 0$ the negative ion signal is due to RET according to the reaction Ar**(ns, nd) + $CCl_4 \rightarrow Ar^+ + Cl^- + CCl_3$. As discussed for the experiments on SF_6 [14,41], the step at $E \approx -3.4$ meV is due to field ionization of Rydberg states with $n^* \gtrsim 63$ (n^* = effective principal quantum number) in the pulsed electric field, used for ion extraction and resulting in a decrease of the effective Rydberg atom density. For quantum numbers $n^* \gtrsim 63$, the effective Rydberg excitation probability at a laser bandwidth of 0.15 meV is essentially constant; therefore the measured negative ion yield directly reflects the n dependence of the rate

coefficients k_{nl} [14,28,29]. In Fig. 2 the dashed line at $E = 0$ corresponds to the $Ar^+(3p^5\ ^2P_{3/2})$ fine structure ionization threshold.

For $E > 0$ the Cl^- yield is proportional to the free electron attachment cross section [14] for the dissociative process (12). It decreases rapidly with increasing electron energy and shows significant structure labeled (a), (b), (c), and (d) in Fig. 2. The energy positions $E_a = 56.9$ meV, $E_b = 113.8$ meV, and $E_c = 170.7$ meV mark the thresholds for excitation of one, two or three quanta of the totally symmetric ν_1 stretch vibration in neutral CCl_4. The downward steps in the cross section are due to coupling between the electron attachment process and the different scattering channels with $^2A_1$ symmetry for the $[CCl_4 + e^-(L = 0)]$ system. An equivalent threshold effect was observed for free electron attachment to SF_6, as reported in [14] and previously predicted theoretically [34]. The downward steps in the CCl_4 data have a somewhat smoother, rounded-off appearance in comparison to the ν_1 feature in SF_6 [14] (some broadening occurs for CCl_4 through the presence of the two isotopes ^{35}Cl and ^{37}Cl). The sharp peak (d) in Fig. 2 ($E_d \approx 177.4$ meV), located close to the excited $Ar^+(3p^5\ ^2P_{1/2})$ fine structure threshold ($E = 177.5$ meV), is strongly affected by reactions involving field-stabilized autoionizing Rydberg atoms $Ar^{**}(^2P_{1/2}\ nl')$:

$$Ar^{**}(^2P_{1/2}nl') + CCl_4 \rightarrow Ar^+ + Cl^- + CCl_3. \quad (13)$$

This effect was discussed in detail in [41]. The total negative ion signal for $E > 177.5$ meV (i.e. $\lambda_2 < 433.3$ nm) results from the superposition of the two attachment reactions (12) and (14):

$$e^-(E' = E - 177.5\ \text{meV}) + CCl_4 \rightarrow Cl^- + CCl_3. \quad (14)$$

Apart from the dominant generation of fast photoelectrons with energy $E[Ar^+(3p^5\ ^2P_{3/2})$ formation] slow electrons with energy $E' = E - 177.5$ meV are produced which are associated with the formation of $Ar^+(3p^5\ ^2P_{1/2})$. The latter channel occurs with much lower probability (about 1%) [14,58], but process (14) clearly stands out at threshold where the attachment cross section is very large. We note that the energy position of the equivalent threshold peak in the SF_6^- data, reported in [14] and Fig. 5 in [41], has to be revised by shifting the peak 0.2 meV to lower energies, as already done in Fig. 8 in [41]. This shift is within the uncertainty of the energy calibration of the data at the $Ar^+(3p^5\ ^2P_{1/2})$ threshold which amounts to 0.2 meV [14,41].

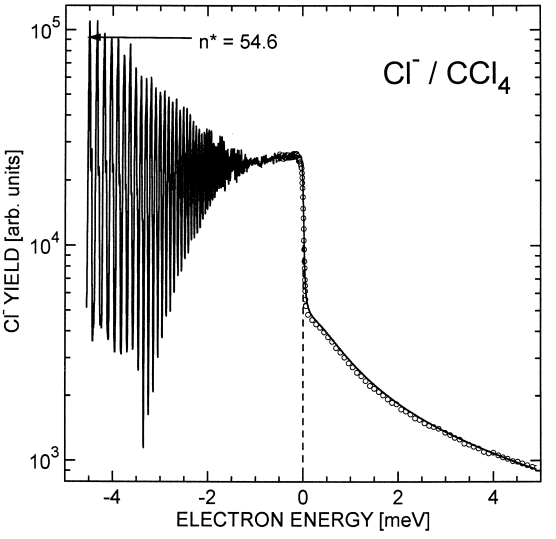

Fig. 3. Cl^- yield due to dissociative attachment to CCl_4 molecules measured over the range from −4.5 to +4.5 meV with a photon energy bandwidth of 0.05 meV (FWHM). The data are compared with model calculations of the attachment yield (smooth line) in which a residual electric field of 0.55 V/m was assumed.

In order to obtain information on the effective residual electric field during the LPA data runs, measurements in a narrow energy range around the $Ar^+(3p^5\ ^2P_{3/2})$ threshold ($E = 0$) were carried out with an optical resolution of about 50 μeV; the result is shown in Fig. 3. As discussed previously in detail for SF_6^- formation [14,41], model calculations of the negative ion yield in the threshold region have been performed, which incorporate the effects of a residual electric stray field with adjustable strength F_s and use the analytical cross section (7) for energies above 0 eV with the parameter β appropriately chosen ($\beta = 0.59(6)\ (\text{meV})^{-1/2}$, see the following) and a constant

negative ion yield at energies below 0 eV, simulating the RET induced Cl^- signal at high principal quantum numbers (see also [41], Eq. (16), and accompanying discussion). The latter is convoluted with the energy profile of the ionizing laser which was deduced from the appearance of RET signals at low principal quantum numbers around $n = 20$; the profile is nearly Gaussian with energy widths of 0.15 meV (without etalon) and 0.05 meV (with etalon in cavity). From the comparison of the measured data with the calculated energy dependence (shown in Fig. 3 as smooth line) an electric stray field of $F_s = 0.55$ V/m was determined. At this field, the classical prediction for the (negative) shift of the ionization threshold $\Delta E_F = 75.9\ \mu\text{eV} \times (F_S[\text{V/m}])^{1/2}$, which amounts to $\Delta E_F = 56\ \mu$eV, is consistent with the experimentally observed (negative) threshold shift of (70 ± 25) μeV, determined relative to the known energy position of the high n Rydberg structure in Fig. 3.

The higher resolution data in Fig. 3 were combined with those in Fig. 2 in order to construct an optimal attachment yield function $Y_e(E)$ which forms the basis for further evaluations. Absolute cross sections $\sigma_e(E)$ for process (12) were obtained from this combined attachment yield $Y_e(E)$ with the procedure outlined above [see Eq. (11)] and are presented in Fig. 4 over the energy range from 0.1 to 2000 meV together with results from other experiments. We use the thermal electron attachment rate coefficient $k_e(T = 300\ \text{K}) = 3.79(19) \times 10^{-7}\ \text{cm}^3\ \text{s}^{-1}$ given by Orient et al. [51] which has a quoted uncertainty of only 5% and agrees well with several other independent determinations (see Table I in [13], Table 1 in [60], and Table 1 in [21]), including the FALP results of Smith et al. [$3.9(5) \times 10^{-7}\ \text{cm}^3\ \text{s}^{-1}$ [50]], Spanel et al. [$3.3(5) \times 10^{-7}\ \text{cm}^3\ \text{s}^{-1}$ [52]], and Burns et al. [$3.6 \times 10^{-7}\ \text{cm}^3\ \text{s}^{-1}$ [21], calibration of apparatus using $k(T = 300\ \text{K}; SF_6) = 2.2 \times 10^{-7}\ \text{cm}^3\ \text{s}^{-1}$] as well as the pulse-radiolysis microwave-cavity based determination of Shimamori et al. [$4.0(5) \times 10^{-7}\ \text{cm}^3\ \text{s}^{-1}$ [13]]. In Fig. 4, the LPA results are shown by the thick line, connecting the original data points in the energy range 0.8–173 meV. Below the first vibrational threshold ($E = 56.9$ meV) our measured cross section is very well described by (7) with the fitted parameters σ_0 and β given in Table 1. This function is represented by the dash-dotted line for

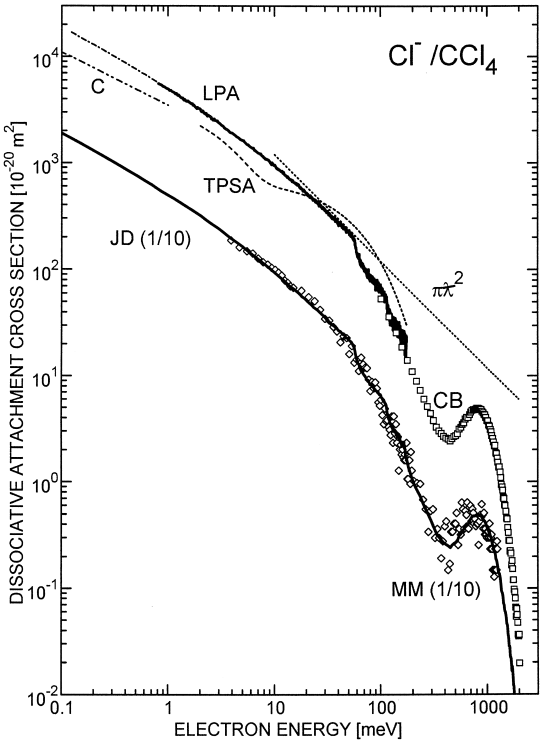

Fig. 4. Absolute cross section for Cl^- formation in free electron attachment to CCl_4 molecules in the energy range from 0.1 to 2000 meV. The overlapping data points (thick line) from 0.8 to 173 meV represent the LPA cross section (energy width ≤1 meV, absolute scale determined by normalization to swarm data, see text); below 0.8 meV the dash-dotted line shows the extrapolation of the fit to the LPA cross section with Eq. (7) and the parameters given in the text and in Table 1. The dotted line shows the s-wave reaction cross section $\pi\lambda\!\!\!^{-2} \propto E^{-1}$. The dash-dot-dot line (C) denotes the capture cross section, equation (5). The dashed line (TPSA) represents VUV photoelectron attachment results [8] (quoted energy width 6 meV, FWHM), according to the fitted cross section (16) with parameters given in the text. The open squares in the range 100–2000 meV, labeled CB, represent electron beam data [25,48]; data points below 100 meV have been omitted in view of the limited experimental resolution (energy width 105 meV, for absolute calibration see text). The cross section curve labeled JD represents the joint LPA and beam [25] data (divided by 10) and is compared with the beam results of Matejcik and co-workers [47,63], which we normalized to the JD cross section at 95 meV (open diamonds, labeled MM; quoted energy width 20 meV for energies above 18 meV and 7 meV (FWHM) for lower energies, data points below 4 meV have been omitted in view of limited resolution, data points above 200 meV have been replaced by their five point average).

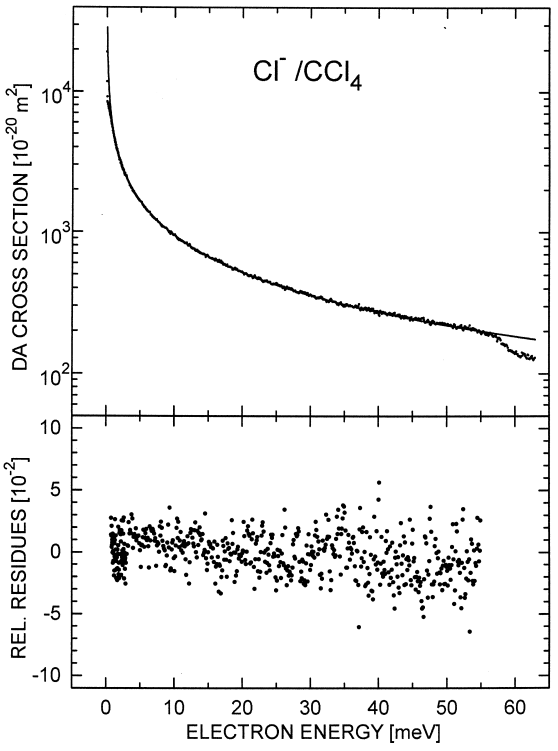

Fig. 5. Comparison of the experimentally determined LPA cross section with the fitted cross section based on the modified Klots formula (7) within the energy range 0.8–55 meV (upper graph). The lower graph shows the relative differences between the fitted and the experimental cross section.

energies below 0.8 meV; between 0.8 and 55 meV, this function cannot be distinguished from the experimental data on the given scale and layout. In order to illustrate the quality of the fit we show in Fig. 5 the DA cross section and the relative difference between the fit function and the data points (lower panel in Fig. 5) over the range 0.8 to 55 meV.

The criterion $\beta^2 E > 0.1$ for "substantial" deviations from the limiting threshold behaviour $\sigma_0 \beta E^{-1/2}$ (see previous discussion) applies for energies $E >$ 0.3 meV, i.e. the limiting *s*-wave law is reached at energies below those experimentally covered. More explicitly, the deviation of the experimental cross section from the limiting *s*-wave behaviour amounts to −24% and −55% at electron energies of $E = 1$ and 10 meV, respectively. The limiting DA rate coefficient, calculated from σ_0 and β, amounts to $k_e(E \rightarrow 0) = 12.3(19) \times 10^{-7}$ cm^3 s^{-1}. While formula (7) is well capable to parametrize the rising slope of the measured decreasing cross section in a simple analytical way for energies up to 55 meV, it also provides a satisfactory description of the absolute cross section at energies below 0.5 meV, as discussed next.

As shown by Dunning and co-workers (Fig. 1 in [56]), good agreement (to within 10%–20%) is obtained between the measured, essentially constant rate coefficients (mean value $k_{nl} = 11(2) \times 10^{-7}$ cm^{-3} [56]) for Cl^- formation in K**(np) + CCl_4 collisions at high n (n = 70–1100, Rydberg electron binding energies 2.8−0.011 meV) with values calculated on the basis of our analytical cross section and the free electron model, Eq. (9). Frey et al. [16,56] also derived absolute attachment cross sections from their RET data through $\sigma_{nl} = k_{nl}/v_M$, using the "median" electron velocity v_M and corresponding effective electron energies from 0.4 down to 0.004 meV, which are much lower than the corresponding Rydberg binding energies (for explanations, see [16,28]). Good agreement between these effective energy dependent RET cross sections with the absolute cross sections given by our analytical fit function (7) is observed (see Fig. 1 in [56] and Fig. 3 in [16]). We note that similarly good agreement also exists between our LPA results and the RET data of Dunning's group for SF_6^- formation (Figs. 2 and 6 in [16]). In view of the independence in the way how the absolute cross sections (rate coefficients) were obtained in the LPA and RET studies this mutual agreement for the two basic molecules SF_6 and CCl_4 establishes a firm platform for their use as benchmark systems in future studies.

Both SF_6 and CCl_4 belong to the few molecules for which the Vogt-Wannier capture model should be applicable in view of missing electric dipole and quadrupole moments, and it is of interest to compare the prediction of the Vogt-Wannier formula (5) with the LPA and the RET data. Assuming the validity of Eq. (5) in the relevant Rydberg electron velocity range one obtains from Eq. (9) with Eq. (5) $k_{nl} = k_c$ where the capture rate coefficient k_c is given by [14]

$$k_c = 7.755 \times 10^{-8}\alpha^{1/2}\ \mathrm{cm^3\ s^{-1}} \quad (15)$$

with α in atomic units of a_0^3. Using $\alpha(SF_6) = 44.1\ a_0^3$ [39] and $\alpha(CCl_4) = 75.6\ a_0^3$ [39], one obtains $k_c(SF_6) = 5.15 \times 10^{-7}\ \mathrm{cm^3\ s^{-1}}$ and $k_c(CCl_4) = 6.74 \times 10^{-7}\ \mathrm{cm^3\ s^{-1}}$. For SF_6, the RET value at high n $k_{nl} = 4.0(10) \times 10^{-7}\ \mathrm{cm^3\ s^{-1}}$ [54] and the LPA result for $k_e(E \rightarrow 0) = 5.4(8) \times 10^{-7}\ \mathrm{cm^3\ s^{-1}}$ [14] are both in satisfactory agreement with the capture rate coefficient k_c. For CCl_4, $k_{nl} = 11(2) \times 10^{-7}\ \mathrm{cm^3\ s^{-1}}$ [56] and the LPA result $k_e(E \rightarrow 0) = 12.3(19) \times 10^{-7}\ \mathrm{cm^3\ s^{-1}}$ are compatible with each other, as discussed above, but they are both distinctly higher than the capture rate coefficient k_c. If the experimental rate coefficients were smaller than the capture rate coefficient, this difference could be explained by pathways (e.g. by reemission of the electron) in which the negative ion complex, formed in the primary capture process, does not form stable (or sufficiently long-lived) negative ions. The opposite finding is more difficult to rationalize and will be discussed with regard to the possible influence of a virtual or weakly bound anion state in a future paper [61].

We now come back to the discussion of Fig. 4. The dashed line represents the attachment cross section determined with the TPSA method by Chutjian and Alajajian from measurements with an estimated energy resolution of 6 meV (FWHM) [8]. We note that the original TPSA data points did not provide evidence for the downward-step like structure in the attachment yield, clearly seen in the LPA data at the onsets for vibrationally inelastic scattering. The following analytical form for the attachment cross section was used to describe the TPSA data over the range from 0 to 140 meV [8,19]:

$$\sigma_{\mathrm{TPSA}}(E) = N[aE^{-1/2}\exp(-E^2/\lambda^2) + \exp(-E/\gamma)]. \quad (16)$$

It contains three fit parameters a, λ, and γ and a normalization constant N; the latter is determined in the same way as for our LPA cross sections [see Eq. (11)]. For the process Cl^-/CCl_4 Chutjian and Alajajian [8] found the values $a = 3.7$, $\lambda = 5.0$, and $\gamma = 56.1$ (energy E in meV) by fitting their measured Cl^- yield with Eq. (16). For a proper comparison with our data we replaced their original normalization constant $N = 545 \times 10^{-20}\ \mathrm{m^2}$ by the value $N = 700 \times 10^{-20}\ \mathrm{m^2}$, thereby accounting for the different, more recent thermal attachment rate coefficient $k_e(T = 300\ \mathrm{K})$ [51], used in this article (see previous discussion and Table 1). Systematic deviations between the LPA and TPSA results are obvious and very similar to those observed and discussed earlier for free electron attachment to SF_6 [14,41]. The TPSA cross section is too small in the range $0 < E < 20$ meV and—correspondingly (normalization to the same thermal rate coefficient)—too large towards higher energies. At low energies the TPSA data appear to exhibit a reduced attachment yield which may be due to the effects of the electric fields continuously present for ion extraction in the TPSA experiment. We also note that the ansatz (16) has the deficiency that the second exponential term (which serves to describe the fast decrease of the cross section at higher energies) is not cut off toward very low energies where the first term (which describes the limiting s-wave behaviour) should take over. As long as the first term is not much larger than the second one, this leads to a more or less substantial perturbation of the s-wave term; at $E = 2$ meV, for example, the first term is only 2.3 times larger than the second one.

In Fig. 4 we have also included the results of recent electron beam experiments [18,25,47]. Chu and Burrow [25] used a magnetically collimated electron beam from a trochoidal monochromator and found, in addition to a resolution limited peak close to 0 eV (FWHM $\approx$ 105 meV), a broader peak centered at 800 meV (FWHM about 660 meV). The peak height of the second peak amounts to 1.9% of the peak at 0 eV; its absolute cross section, recently determined with reference to CCl_3H [25,48,62], amounts to $4.95 \times 10^{-20}\ \mathrm{m^2}$ ($\pm$30%). In Fig. 4 we have included the absolute beam cross sections (open squares) over the range from 0.1 to 2.0 eV [48] (the energy scale of the original data [25] has been shifted by +23 meV for reasons explained in the Appendix). The smooth line in Fig. 4, denoted as JD (joint data), represents a combination of our LPA results (ten point average)

with the absolute cross section data of Burrow [48] with suitable interpolation between 173 and 238 meV. For clarity of presentation, the JD cross section has been multiplied by (1/10). It is compared with the beam data of Matejcik et al. (open diamonds, results from Fig. 6 in [47], augmented by points at higher energies [63], quoted energy width 20 meV) which are normalized to the JD cross section at $E = 85$ meV. Matejcik and co-workers used an improved trochoidal electron monochromator, capable of resolutions down to about 7 meV, and detected Cl^- ions with a quadrupole mass spectrometer (for energies above about 0.6 eV the Cl^- yield starts to be smaller than the total attachment cross section because of the production of the other fragment ions [10], see above). Due to the improved resolution Matejcik et al. found the height of the peak at higher energy to be only 0.3% [18] and 0.16% [47] relative to their zero energy peak. For the JD data set, the ratio of the cross section at 800 meV relative to those at 10 and 1 meV amounts to 0.53% and 0.10%, respectively (In the Appendix, we quote ratios of the cross section at 800 meV relative to that at the zero energy peak for different experimental resolutions). Satisfactory overall agreement is found between the JD cross section and the results of Matejcik et al. [47,63], but there is no clear evidence in these beam data for the sharp downward-steplike decrease in the attachment cross section at the onsets for vibrationally inelastic scattering.

We mention that we did not include in Fig. 4 the cross section, derived from analyses of electron swarm data in conjunction with deconvolution techniques and reported by Christophorou et al. (Fig. 31 in [64], see also Fig. 19, upper right in [65]). This unfolded cross section exhibits—in substantial contrast to the trend of the LPA cross section and to the electron beam data [18,25,47]—a distinct peak at an energy of about 0.2 eV. We attribute this peak to problems in the deconvolution procedure of the swarm data; note that even weak shoulders in the original swarm data as a function of mean electron energy can result in a peak in the unfolded energy dependent cross section.

In view of its high resolution and good statistical quality we recommend to use the JD cross section as benchmark data for future low energy DA work. The JD cross section may, e.g. be used to construct the energy dependent cross section for backward electron scattering from CCl_4 by subtracting it from the cross section reported by Randell et al. [66]. Measuring the transmission of a magnetically confined electron beam (quoted width 5.5 meV) through a static scattering cell, these authors obtained the sum of the cross sections for backward electron scattering and electron attachment. At low energies, the energy dependence of their cross section, which does not show specific structure, can be approximately represented by $\sigma_R \propto E^{-0.9}$. Randell et al. established an absolute scale by normalizing their relative data to the Klots cross section at $E = 10$ meV which is somewhat lower than our LPA cross section.

3.2. Energy dependent rate coefficients for electron attachment to CCl_4

In Fig. 6 we present the energy dependent LPA rate coefficient $k_e(E)$ over the range (0.8–173) meV. Our limiting value $k_e(E \rightarrow 0) = 12.3(19) \times 10^{-7}$ cm^3 s^{-1} (full circle) is in good agreement with the most recent rate coefficients $k_{nl} \approx 11(2) \times 10^{-7}$ cm^3 s^{-1} [56] for RET in K**(np) + CCl_4 collisions at high principal quantum numbers ($n \geq 70$), already quoted above (note that this value replaces the somewhat lower number 8.5(20) $\times 10^{-7}$ cm^3 s^{-1} determined by Ling et al. [54], see also the discussion in the survey article of Dunning [16]). Toward higher electron energies $k_e(E)$ decreases substantially, and one might expect to see this decrease reflected in a certain drop of the RET rate coefficients k_{nl} toward smaller n. The data of the Rice group [16,27,54] appear to be compatible with such a trend, but results with smaller uncertainties in the n dependent Rydberg rate coefficients are needed to confirm this expectation. We note that effects of postattachment interactions in the final state ionic complex, formed in RET toward lower n, have to be carefully considered for a meaningful comparison of measured rate coefficients with k_{nl} values derived from $k_e(E)$ on the basis of quasifree electron model.

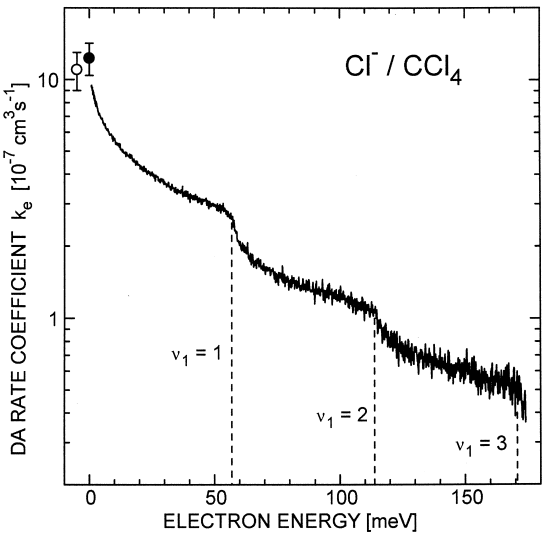

Fig. 6. Energy dependence of the electron attachment rate coefficient $k_e(E) = \sigma_e(E)v_e$ for Cl^- formation to CCl_4 over the range 0.8–173 meV. The open circle with error bars (displaced from $E = 0$ eV for clarity) represents the rate coefficient for Rydberg electron attachment to CCl_4 molecules at high principal quantum numbers [16,56], see text. The closed circle represents the rate coefficient for threshold electron attachment $k_e(E \rightarrow 0)$ which corresponds to the extrapolated, limiting LPA cross section (see text). The vertical dashed lines denote the onsets for vibrational excitation of one, two, and three quanta of the symmetric stretch vibrational mode.

As compared to their appearance in Figs. 2 and 4, the downward steps at the onsets for excitation of one ($\nu_1 = 1$), two ($\nu_1 = 2$), and three quanta ($\nu_1 = 3$) of the symmetric stretch vibration appear to be clearer in the plot of the DA rate coefficient $k_e(E)$ in Fig. 6. The vertical dashed lines at the three vibrational onsets label the respective energy positions, determined by Raman spectroscopy. So far, no theoretical calculations for DA involving CCl_4 are available to our knowledge. Normally, DA calculations assume prompt dissociation of the temporary negative ion formed in the primary electron attachment process; this assumption cannot be made for CCl_4, however, as indicated by detailed analyses of Cl^- production from K**(np) + CCl_4 collisions at low and high principal quantum numbers by Popple et al. [55]. These authors measured the angular and velocity distribution of the Cl^- ions resulting from the RET process with velocity selected K**(np) atoms. Information on the decay energetics of the CCl_4^{-*} intermediate was obtained from measurements at high n ($n = 55$) where electrostatic interactions (postattachment effects) between the product ions are negligible. Studies at low n ($n = 14$) in conjunction with Monte Carlo modeling of the reaction kinematics yielded information on the lifetime of the intermediate which was determined to be 7.5(25) ps [55] with the consequence that only a small fraction of the available excess energy of reaction (here about 0.6 eV) appears as translational energy. As mentioned in Sec. 2, this finding (if applicable also to free electron attachment at low energy) suggests that possible discrimination effects associated with variations of product kinetic energy as a function of electron energy [see Eq. (2)] are negligible for DA to CCl_4.

Using the recommended JD cross section (see Fig. 4), we calculated thermal DA rate coefficients $k_e(T_e)$ for fixed gas temperature $T_G = 300$ K as a function of electron temperature T_e. In Fig. 7 the results are compared with two sets of swarm data, obtained by Shimamori et al. [13] with a microwave cavity pulse radiolysis–microwave heating (MWPR–MH) method and by Spanel et al. [52] with a flowing afterglow/Langmuir probe (FALP) apparatus involving an electron swarm with a variable temperature [52]. We note that the respective rate coefficients at $T = T_e = T_G = 300$ K agree within their mutual experimental uncertainties: LPA calibration: $3.79(9) \times 10^{-7}$ cm^3 s^{-1}; MWPR–MH: $4.0(5) \times 10^{-7}$ cm^3 s^{-1}; FALP: $3.3(5) \times 10^{-7}$ cm^3 s^{-1}. Good overall agreement with regard to the dependence on electron temperature is observed between the calculated results and the swarm data although it appears that the drop in the rate coefficients towards higher temperatures is somewhat slower in the FALP data than in both the LPA derived and in the MWPR–MH results. Possibly, the electron energy distribution in the FALP method [52] at the elevated electron temperatures is somewhat lower than assigned. We note that this is the first time that reliable electron beam-derived rate coefficients for dissociative attachment are compared with swarm data over such an extended range of electron temperature (at the fixed gas temperature of $T_G = 300$ K). We emphasise that it is important that the beam data

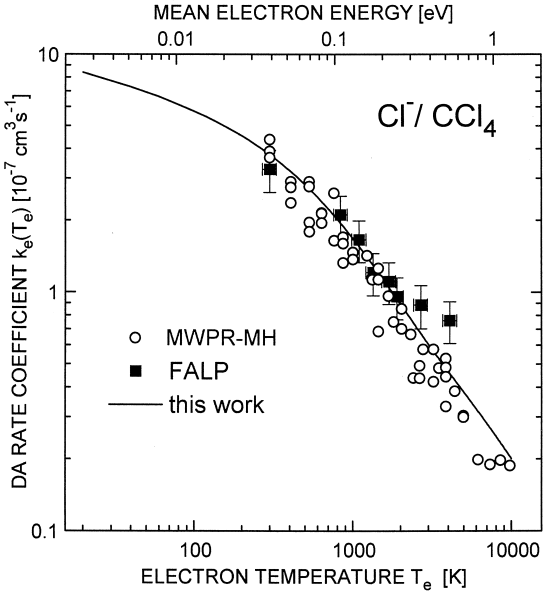

Fig. 7. Thermal rate coefficient $k_e(T_e)$ for electron attachment to CCl_4 molecules as a function of electron temperature T_e for a Maxwellian electron energy distribution and constant gas temperature $T_G = 300$ K. The solid line represents rate coefficients for $T_e = 30$–10 000 K calculated on the basis of the recommended total electron attachment cross section labelled JD in Fig. 4. The open circles and closed squares present the swarm results, obtained with the MWPR–MH [13] and the temperature variable FALP method [52], respectively.

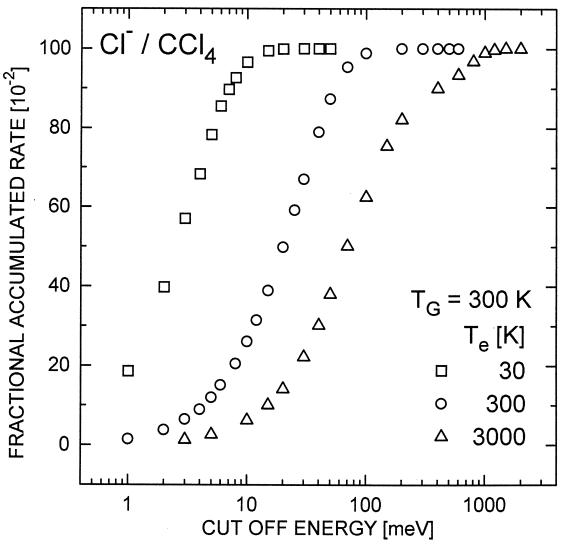

Fig. 8. Fraction of the accumulated rate coefficient $k_{acc}(E)$ relative to the total rate coefficient $k_e(T_e, T_G = 300\ \text{K})$ for three Maxwellian electron distributions with temperatures of $T_e = 30$ K (open squares), $T_e = 300$ K (open circles), and $T_e = 3000$ K (open triangles) (see text).

include results obtained with very high (meV) resolution in order to avoid uncertainties associated with the true behaviour of the attachment cross section at the lowest energies. In this connection we mention that about 60% of the total rate coefficient $k_e(T_e = T_G = 300\ \text{K})$ stem from electrons with energies $E \leq 25.85$ meV (i.e. energies below the thermal energy k_BT at $T = 300$ K). For illustration, we present in Fig. 8 the percent fraction $k_{acc}(E)/k_e(T_e = T_G = 300\ \text{K})$ of the accumulated rate coefficient $k_{acc}(E)$, defined by [14]

$$k_{acc}(E) = \int_0^E k_e(E')\, f(E')\, dE'. \tag{17}$$

At $E = 20$ meV, $k_{acc}(E)$ amounts to 50% of the full value while for energies up to the mean electron energy $E = (3/2)k_BT_e = 38.8$ meV at $T_e = 300$ K, $k_{acc}(E)$ reaches 78% of the total value. For comparison we mention that for electron attachment to SF_6 the 50% value of $k_{acc}(E)/k_e(T_e = T_G = 300\ \text{K})$ is reached at $E = 22.3$ meV [14]; this slightly higher value as compared to CCl_4 reflects the fact that the value of β is smaller for SF_6 than for CCl_4 (see previous discussion). Toward lower electron temperatures, the contributions from energies below 10 meV become increasingly important. For illustration we have included in Fig. 8 the fraction $k_{acc}(E)/k_e(T_e = 30\ \text{K}, T_G = 300\ \text{K})$ at an electron temperature of 30 K while the gas temperature is kept at $T_G = 300$ K. The 50% value of $k_{acc}(E)$ is reached at $E = 2.6$ meV. The contribution to $k_{acc}(E)$ from energies at which our cross section relies on the extrapolation formula (7) becomes substantial at these low electron temperatures [$k_{acc}(E = 1\ \text{meV})/k_e(T_e = 30\ \text{K}, T_G = 300\ \text{K}) = 18.6\%$]. On the other hand, for the highest temperature example $T_e = 3000$ K shown in Fig. 8, the contributions from electron energies $E \geq 173$ meV (beyond the energy range of our experiment) amount to only 20% of the total thermal rate.

It would be interesting to have available DA cross

sections of comparable quality as those reported here for CCl_4 at $T_G = 300$ K at several other gas temperatures and for molecules which exhibit vastly different variations of the rate coefficients $k_e(T)$ as a function of the global temperature $T = T_e = T_G$ [15]. For CCl_4, swarm data of Smith et al. [50] and Burns et al. [21], carried out with two variants of the FALP method in the temperature range $T = 200$ K to 800 K, indicate that the rate coefficients $k_e(T)$ decrease toward higher temperatures, but the quantitative trends in the two data sets are quite different: Smith et al. [50] find a continuous decrease from 4.1×10^{-7} cm^3 s^{-1} at $T = 205$ K to 3.5×10^{-7} cm^3 s^{-1} at $T = 590$ K, while Burns et al. [21] report a much faster falloff from 3.6×10^{-7} cm^3 s^{-1} at $T = 293$ K via 1.4×10^{-7} cm^3 s^{-1} at $T = 590$ K to 1.2×10^{-7} cm^3 s^{-1} at $T = 777$ K. Burns et al. normalize their rate coefficients at each temperature to those for attachment to SF_6 and assume that $k_e(T; SF_6) = 2.2 \times 10^{-7}$ cm^3 s^{-1} is independent of the temperature T over the range of interest. This assumption is supported by swarm data of Fehsenfeld [67] and Petrovic and Crompton [7] as well as by electron beam work of Spence and Schulz [2] who found the total, energy integrated cross section for formation of negative ions in low energy electron collisions with SF_6 to be independent of gas temperature within the range $T_G = 300$–1200 K. Spence and Schulz [2] found essentially the same behaviour for CCl_4; this trend is in line with the weak variation of $k_e(T)$ reported by Smith et al. [50], but in contrast to the observations of Burns et al. [21]. Further experimental investigations are needed to clarify the situation.

4. Conclusions

Using the LPA method at an energy width of 1 meV, we have determined absolute cross sections for dissociative electron attachment to the CCl_4 molecule over the electron energy range $0.8 \leq E \leq 173$ meV. At thresholds for vibrational excitation of the neutral molecule, the cross section exhibits pronounced, previously unobserved cusp structure of downward step character due to coupling of the attachment process with scattering channels. At energies below these onsets the cross section is well described by the empirical formula $\sigma_e(E) = (\sigma_0/E)[1 - \exp(-\beta E^{1/2})]$, where β takes the value 0.59(6) $(meV)^{-1/2}$. Thus the threshold behaviour of the cross section $\sigma_e(E) \propto E^{-1/2}$, theoretically predicted for s-wave attachment to molecules without permanent electric dipole moment, is approximately reached at very low energies ($E \lesssim 0.3$ meV). As found and discussed before for SF_6, the cross sections derived from previous photoelectron attachment work (TPSA) deviate substantially from the present work. Lower resolution work with electron beams and swarms is also compared with the LPA data. A joint LPA-beam data set is obtained over the range 0–2 eV which we recommend to use as total electron attachment cross section for the CCl_4 molecule and as benchmark cross section in future low energy electron attachment studies. Based on this cross section, we calculate and report the energy dependence of the rate coefficients $k_e(E)$ for monoenergetic free electron attachment and the electron temperature dependence of the rate coefficients $k_e(T_e)$ for free electron attachment involving a Maxwellian electron ensemble and a gas at room temperature ($T_G = 300$ K). The LPA result for the limiting value $k_e(E \rightarrow 0)$ is found to be in good agreement with the rate coefficient k_{nl} for Rydberg electron attachment at high principal quantum numbers [16]; these values are both significantly higher than the rate coefficient $k_c(E \rightarrow 0)$ for electron capture through the static polarization interaction between the electron and the CCl_4 molecule.

Acknowledgements

This work has been supported by the Deutsche Forschungsgemeinschaft through Sonderforschungsbereich 91 *Energietransfer bei Atomaren und Molekularen Stossprozessen*, Schwerpunktprogramm *Molekulare Cluster* and Forschergruppe *Niederenergetische Elektronenstreuprozesse*. The authors gratefully acknowledge P. D. Burrow, H. Shimamori, S. Matejcik, G. Senn, and T. D. Märk for providing data in numerical form. They thank R. W. Crompton for

communicating unpublished results and P. D. Burrow, L. G. Christophorou, I. I. Fabrikant, and A. Schramm for useful comments. This work is based in part on the unpublished dissertation, Univ. Kaiserslautern, of one of the authors (D.K.).

Appendix

We discuss in some detail the effects of the finite energy width on measured electron attachment cross sections for the CCl_4 molecule, in particular, in regions over which the cross section varies strongly, e.g. close to zero energy and around vibrational onsets. We note that electron attachment to CCl_4 has been recently used by the Innsbruck group (see, e.g. [47]), to obtain information on the effective energy width in their electron attachment experiments. For clarity we distinguish between the true DA cross section $\sigma_e(E)$ (represented by the JD cross section in Fig. 4) and the measured DA yield function $Y(U)$ which represents an effective cross section resulting from the convolution of the electron energy distribution function $f(U - E)$ (whose integral over energy is assumed to be normalized to 1) with the cross section [68], i.e.

$$Y(U) = \int \sigma_e(E)\, f(U - E)\, dE. \qquad (18)$$

The energy U denotes the peak energy of the distribution function to which the experimental apparatus has been set. Although experimental electron energy distribution functions are often not symmetrical (see, e.g. the analysis of electron attachment data for C_{60} and C_{70} in the Appendix of [68]) we use a normalized Gaussian function for simplicity. Qualitatively one expects that the convolution of a Gaussian (energy width ΔE_{FWHM}) with an integrable divergence at zero energy [such as the LPA fit cross section of the form Eq. (7)] results in a peak which appears at an effective energy U_p slightly above zero and a width ΔU_{FWHM} somewhat broader than ΔE. Apart from the peak position U_p and the width ΔU of the "zero energy peak," another aspect of interest is the energy range

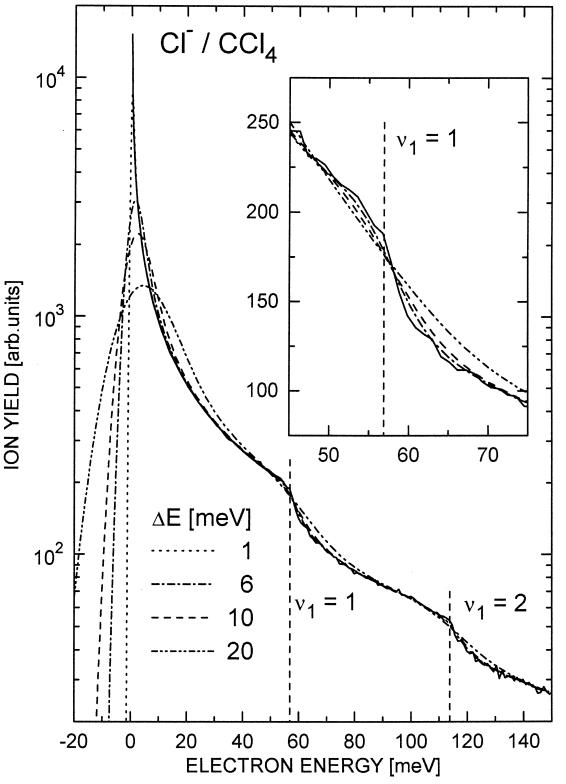

Fig. 9. Effects of energy resolution on measured dissociative electron attachment yields for the CCl_4 molecule, as obtained by convoluting the recommended DA cross section (solid line) with Gaussian electron energy distributions of widths ΔE_{FWHM} of 1, 6, 10, and 20 meV, respectively (see text). The downward step structure at the onset for vibrational excitation of the $\nu_1 = 1$ mode is shown in the insert on expanded linear scales.

over which the finite experimental energy width causes significant deviations of the measured yield $Y(U)$ from the true cross section function $\sigma_e(U)$.

In Figs. 9 and 10 we show several examples of yield functions $Y(U)$, obtained by convolution of the true DA cross section for CCl_4 with Gaussians with widths ΔE_{FWHM} of 1, 6, 10, 20 and 20, 50, 100, 200 meV, respectively. In order to handle the singularity at zero energy as precisely as possible, the recommended cross section (JD) has been replaced by the modified Klots formula Eq. (7) below $E = 45$ meV (see Fig. 5) and arranged into 0.2 meV bins ($E_i \pm 0.1$ meV): for $E \leq 4$ meV, the respective integrals of Eq. (7) over these 0.2 meV intervals have been set at E_i

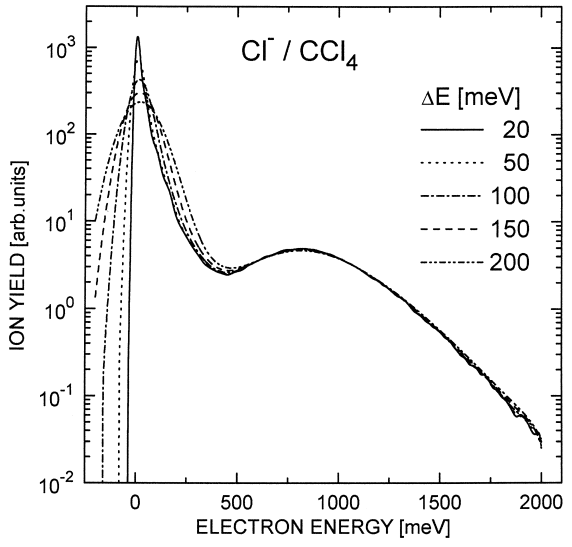

Fig. 10. Effects of energy resolution on measured dissociative electron attachment yields for the CCl_4 molecule, as obtained by convoluting the recommended DA cross section with Gaussian electron energy distributions of widths ΔE_{FWHM} of 20, 50, 100, 150, and 200 meV, respectively (see text).

(for $E_i = 0$, the integral from 0 to 0.1 meV has been taken); for $E > 4$ meV, the values of Eq. (7) at E_i are nearly identical to the respective integrals. The resulting true cross section, shown as full line in Fig. 9, has been the basis for calculating the convoluted cross section for $\Delta E = 1$ meV. Then, the $\Delta E = 1$ meV curve ($0 \leq E \leq 55$ meV) and the data set JD ($55 < E \leq 2000$ meV) have been the basis for calculating the other convoluted cross sections shown in Figs. 9 and 10. For energies U below (*above*) about 1.5 U_p, the yield functions $Y(U)$ stay below (*above*) the true cross section. At some higher energy points U_m, the yield functions $Y(U)$ match the true cross section, depending on the energy widths ΔE in a more difficult way (due to the cusp structures and the minimum between the zero energy peak and the second peak at 800 meV) so that no simple relation can be established between U_p and U_m. The sharp downward step structure at the onsets for vibrational excitation of the symmetric stretch mode ($\nu_1 = 1$, $\nu_1 = 2$) can be clearly seen even at an energy width of 10 meV if data are taken with good statistical accuracy (but barely at a width of 20 meV, see insert in Fig. 9 for the $\nu_1 = 1$ threshold). In Table 2 we summarize the results obtained for the effective peak positions U_p and the effective widths ΔU_{FWHM} as a function of the experimental energy width ΔE_{FWHM}. We note that the peak shift of the zero energy peak has been neglected in most of the previous work. This shift is intrinsically related to the asymmetry of the cross section which only exists for positive values of the energy while the energy U (tuned by a voltage) can take negative values. Note that the convolution of symmetrical sharp structure in the cross section, centered at higher energies around the value U_r will yield peak locations U_p which agree with U_r. In contrast asymmetrical structure such as the vibrational Feshbach resonance

Table 2
Effects of energy resolution on the true cross section for electron attachment to CCl_4

Experimental electron energy resolution ΔE_{FWHM} (meV)	Apparent peak position of zero energy peak U_p (meV)	Apparent width of zero energy peak ΔU_{FWHM} (meV)	Apparent cross section of zero energy peak (10^{-20} m^2)	Apparent cross section ratio of second peak at 0.8 eV (10^{-2})
1	0.3	1.7	8800	0.056
6	1.5	8.5	3106	0.16
10	2.3	13.7	2240	0.22
20	4.1	26	1413	0.35
30	5.6	38	1058	0.47
50	8.5	61	730	0.67
70	11.0	82	567	0.86
100	13.5	113	425	1.14
150	17	163	302	1.58
200	19	213	236	1.98

at about $E = 60$ meV in DA to CH_3I (yielding I^- ions) and followed by a strong sharp decrease of the cross section on the high energy side will result in peak shifts and asymmetrical broadening upon convolution (see [30]).

In Table 1 we list also energy integrated cross sections derived from our recommended data for electron attachment to CCl_4 (as well as for SF_6) which are helpful quantities when comparing cross section data of different quality with respect to energy resolution. Our results for both molecules are larger than those presented by Spence and Schulz [2] by factors of 1.25 (SF_6) and 3.5 (CCl_4). Note, however, that the data in [2] were normalized in absolute value to swarm data which are superseded by more recent work, in particular the results presented in this article.

References

[1] G.J. Schulz, Rev. Mod. Phys. 45 (1973) 423.
[2] D. Spence, G.J. Schulz, J. Chem. Phys. 58 (1973) 1800.
[3] H.S.W. Massey, Negative Ions, Cambridge University Press, Cambridge, 1976.
[4] L.G. Christophorou, Adv. Electron. Electron Phys. 46 (1978) 55.
[5] R.N. Compton, in Electronic and Atomic Collisions, N. Oda, K. Takayanagi (Eds.), North-Holland, Amsterdam, 1980) p. 251.
[6] Electron–Molecule Interactions and their Applications, L.G. Christophorou (Ed.), Academic, New York, 1984, Vols. 1 and 2.
[7] Z.Lj. Petrovic, R.W. Crompton, J. Phys. B 18 (1985) 2777.
[8] A. Chutjian, S.H. Alajajian, Phys. Rev. A 31 (1985) 2885.
[9] Y. Hatano, in Electronic and Atomic Collisions, D.C. Lorents, W.E. Meyerhof, J.R. Peterson (Eds.), North-Holland, Amsterdam, 1986, p. 153.
[10] T. Oster, A. Kühn, E. Illenberger, Int. J. Mass Spectrom. Ion Processes 89 (1989) 1.
[11] W. Domcke, Phys. Rep. 208 (1991) 97.
[12] A. Chutjian, in Electronic and Atomic Collisions, W.R. MacGillivray, I.E. McCarthy, M.C. Standage (Eds.), Adam Hilger, Bristol, 1992, pp. 127–138.
[13] H. Shimamori, Y. Tatsumi, Y. Ogawa, T. Sunagawa, Chem. Phys. Lett. 194 (1992) 223.
[14] D. Klar, M.-W. Ruf, H. Hotop, Chem. Phys. Lett. 189 (1992) 448; Aust. J. Phys. 45 (1992) 263.
[15] D. Smith, P. Spanel, Adv. At. Mol. Opt. Phys. 32 (1994) 307.
[16] F.B. Dunning, J. Phys. B: At. Mol. Opt. Phys. 28 (1995) 1645.
[17] H. Hotop, D. Klar, J. Kreil, M.-W. Ruf, A. Schramm, J.M. Weber, in The Physics of Electronic and Atomic Collisions, L.J. Dubé, J.B.A. Mitchell, J.W. McConkey, C.E. Brion (Eds.), AIP Conf. Proc. 360 (1995) 267.
[18] S. Matejcik, A. Kiendler, A. Stamatovic, T.D. Märk, Int. J. Mass Spectrom. Ion Processes 149/150 (1995) 311.
[19] A. Chutjian, A. Garscadden, J.M. Wadehra, Phys. Rep. 264 (1996) 393.
[20] O. Ingólfsson, F. Weik, E. Illenberger, Int. J. Mass Spectrom. Ion Processes 155 (1996) 1.
[21] S.J. Burns, J.M. Matthews, D.L. McFadden, J. Phys. Chem. 100 (1996) 19436.
[22] J.L. Lebarrec, O. Sidko, J.L. Queffelec, S. Hamon, J.B.A. Mitchell, B.R. Rowe, J. Chem. Phys. 107 (1997) 54.
[23] J.P. Ziesel, I. Nenner, G.J. Schulz, J. Chem. Phys. 63 (1975) 1943.
[24] R. Abouaf, D. Teillet-Billy, J. Phys. B 10 (1977) 2261.
[25] S.C. Chu, P.D. Burrow, Chem. Phys. Lett. 172 (1990) 17.
[26] P.D. Burrow, G.A. Gallup, I.I. Fabrikant, K.D. Jordan, Aust. J. Phys. 49 (1996) 403.
[27] F.B. Dunning, J. Phys. Chem. 91 (1987) 2244.
[28] D. Klar, B. Mirbach, H.J. Korsch, M.-W. Ruf, H. Hotop, Z. Phys. D 31 (1994) 235.
[29] A. Schramm, J.M. Weber, J. Kreil, D. Klar, M.-W. Ruf, H. Hotop, Phys. Rev. Lett. 81 (1998) 778.
[30] A. Schramm, I.I. Fabrikant, J.M. Weber, E. Leber, M.-W. Ruf, H. Hotop, J. Phys. B 32 (1999) 2153.
[31] E.P. Wigner, Phys. Rev. 73 (1948) 1002.
[32] A.I. Baz', Sov. Phys. JETP 6 (1958) 709.
[33] J. Gauyacq, A. Herzenberg, Phys. Rev. A 25 (1982) 2959.
[34] J. Gauyacq, A. Herzenberg, J. Phys. B 17 (1984) 1155.
[35] J. Horácek, W. Domcke, Phys. Rev. A 53 (1996) 2262.
[36] J. Horácek, W. Domcke, H. Nakamura, Z. Phys. D 42 (1997) 181.
[37] E. Vogt, G.H. Wannier, Phys. Rev. 95 (1954) 1190.
[38] C.E. Klots, Chem. Phys. Lett. 38 (1976) 61.
[39] T.M. Miller, in CRC Handbook of Chemistry and Physics, 76th ed., D.R. Lide (Ed.), CRC Press, Boca Raton, FL, 1995, Vol. 10, pp. 192–206.
[40] I.I. Fabrikant, Sov. Phys. JETP 46 (1977) 693.
[41] D. Klar, M.-W. Ruf, H. Hotop, Meas. Sci. Technol. 5 (1994) 1248.
[42] T. Kondow, J. Phys. Chem. 91 (1987) 1307.
[43] T. Kraft, M.-W. Ruf, H. Hotop, Z. Phys. D 14 (1989) 179.
[44] H.S. Carman Jr., C.E. Klots, R.N. Compton, J. Chem. Phys. 99 (1993) 1734.
[45] C. Desfrancois, H. Abdoul-Carime, J.-P. Schermann, Int. J. Mod. Phys. B 12 (1996) 1339.
[46] M. Matsuzawa, J. Phys. Soc. Jpn. 33 (1973) 1108.
[47] S. Matejcik, G. Senn, P. Scheier, A. Kiendler, A. Stamatovic, T.D. Märk, J. Chem. Phys. 107 (1997) 8955.
[48] P.D. Burrow, private communication (1999).
[49] A.A. Christodoulides, L.G. Christophorou, J. Chem. Phys. 54 (1971) 4691.
[50] D. Smith, N.G. Adams, E. Alge, J. Phys. B 17 (1984) 461.
[51] O.J. Orient, A. Chutjian, R.W. Crompton, B. Cheung, Phys. Rev. A 39 (1989) 4494.
[52] P. Spanel, S. Matejcik, D. Smith, J. Phys. B 28 (1995) 2941.
[53] K. Harth, M.-W. Ruf, H. Hotop, Z. Phys. D 14 (1989) 149.

[54] X. Ling, B.G. Lindsay, K.A. Smith, F.B. Dunning, Phys. Rev. A 45 (1992) 242.
[55] R.A. Popple, C.D. Finch, K.A. Smith, F.B. Dunning, J. Chem. Phys. 104 (1996) 8485.
[56] M.T. Frey, S.B. Hill, K.A. Smith, F.B. Dunning, I.I. Fabrikant, Phys. Rev. Lett. 75 (1995) 810.
[57] J.M. Weber, E. Leber, M.-W. Ruf, H. Hotop, Phys. Rev. Lett. 82 (1999) 516.
[58] S. Schohl, D. Klar, N.A. Cherepkov, I.D. Petrov, K. Ueda, S. Baier, R. Kau, H. Hotop, J. Phys. B 30 (1997) 609.
[59] T. Shimanouchi, Tables of Molecular Frequencies, US GPO, Washington, DC, 1972, Vol. I, p. 39.
[60] L.G. Christophorou, Z. Phys. Chem. 195 (1996) 195.
[61] I.I. Fabrikant, H. Hotop, Phys. Rev. A(submitted).
[62] K. Aflatooni, P.D. Burrow, J. Chem. Phys., 113 (2000) 1455.
[63] T.D. Märk, G. Senn, S. Matejcik, private communication, 1999.
[64] L.G. Christophorou, D.L. McCorkle, A.A. Christodoulides, in Electron–Molecule Interactions and Their Applications, L.G. Christophorou, (Ed.), Academic, New York, 1984, Vol. I, pp. 477–617.
[65] L.G. Christophorou, Chem. Rev. 76 (1976) 409.
[66] J. Randell, J.-P. Ziesel, S.L. Lunt, G. Mrotzek, D. Field, J. Phys. B 26 (1993) 3423.
[67] F.C. Fehsenfeld, J. Chem. Phys. 53 (1970) 2000.
[68] J.M. Weber, M.-W. Ruf, H. Hotop, Z. Phys. D 37 (1996) 351.